J Nanopart Res (2019) 21: 52
https://doi.org/10.1007/s11051-019-4491-8

RESEARCH PAPER

Manganese oxides/N-doped carbon particles with high capacity retention for aqueous rechargeable zinc battery

Dong-Shuai Li · Shan Wu · Yi-Fan Wang · Ming Sun · Wei-Liang Liu · Man-Man Ren · Fan-Gong Kong · Shou-Juan Wang · Xin-Qiang Wang

Received: 24 October 2018 / Accepted: 18 February 2019 / Published online: 9 March 2019

Abstract Manganese dioxide as the electrode for aqueous zinc-ion batteries (AZIBs) is influenced by the material dissolution. Herein, β-MnO_2/N-doped carbon matrix (NCm) or Mn_5O_8/NCm composites were fabricated by effective synthesis process using polyaniline (PANI) as carbon/nitrogen sources. The conductive N-doped carbon layer was tied to β-MnO_2, which increased the electrical conductivity of the β-MnO_2 nanorod. At current densities of 200 mA g^{-1}, the β-MnO_2/NCm electrode delivered a higher discharge capacity of 331 mAh g^{-1} comparing with 185 mAh g^{-1} for the pure β-MnO_2 electrode. Besides, the Mn_5O_8/NCm electrode could provide a discharge capacity of 266 mAh g^{-1}. Therefore, the approach in this study may pave the way on preparing manganese oxides/NCm materials for AZIBs.

Keywords Manganese oxide · N-doped · Cathode materials · Capacity retention · Mild aqueous electrolyte · Energy storage

Introduction

New electrical energy storage systems have drawn a tremendous amount of attention as the excellent method to overcome the shortcomings associated with the storage and use of renewable energy (Lund 2007; Jiang et al. 2012; Zhai et al. 2011; Hu et al. 2016). Due to high energy density and long cycling life, lithium-ion batteries have dominated the worldwide battery market for digital and mobile devices (Qiu et al. 2018a, b; Suo et al. 2015; Dunn et al. 2011; Chang et al. 2010; Zhang et al. 2018;

Electronic supplementary material The online version of this article (https://doi.org/10.1007/s11051-019-4491-8) contains supplementary material, which is available to authorized users.

D.-S. Li · S. Wu · Y.-F. Wang · M. Sun · W.-L. Liu (✉) · M.-M. Ren
School of Materials Science and Engineering, Key Laboratory of Amorphous and Polycrystalline Materials, Key Laboratory of Processing and Testing Technology of Glass Functional Ceramics of Shandong Province, Qilu University of Technology (Shandong Academy of Sciences), Daxue Road, Western University Science Park, Jinan 250353, People's Republic of China
e-mail: wlliu@sdu.edu.cn

F.-G. Kong (✉) · S.-J. Wang
State Key Laboratory of Biobased Material and Green Papermaking, Key Laboratory of Pulp & Paper Science and Technology of Shandong Province/Ministry of Education, Qilu University of Technology (Shandong Academy of Sciences), Jinan 250353, People's Republic of China
e-mail: kfg@qlu.edu.cn

X.-Q. Wang
State Key Laboratory of Crystal Materials, Shandong University, Jinan 250100, People's Republic of China

Zhang et al. 2018). However, the high cost and potential safety problems can limit their large-scale applications (Tarascon and Armand 2001; Wang et al. 2013a, b; Bruce et al. 2012; Hu et al. 2017; Wu et al. 2018a, b). Nonetheless, a long lifetime, as well as high energy density, remains a primary dispute (Cao et al. 2017).

During the past decade, a string of aqueous zinc-ion batteries (AZIBs) cathode that can achieve reversibly aqueous zinc-ion storage, for instance, tunnel-type MnO_2 (Alfaruqi et al. 2015a, b; Zhao et al. 2018; He et al. 2017; Boeun Lee et al. 2016), Prussian blue analogues (Trocoli and La Mantia 2015; Zhang et al. 2015), and vanadium oxides (Xia et al. 2018a, b; Yan et al. 2018; Senguttuvan et al. 2016; Sambandam et al. 2018; Hu et al. 2018; Wei et al. 2018) have been reported. Xu et al. assembled a $MnO_2/ZnSO_4$ or $Zn(NO_3)_2/Zn$ system, which contributed a high discharge capacity of 210 mAh g^{-1} (Xu et al. 2012). Additionally, graphene scroll-coated α-MnO_2 nanowires have been studied as cathodes materials, which demonstrated high capacity, outstanding rate performance and distinguished stable storage (Wu et al. 2018a, b). Besides, the graphene oxide scrolls reduced the dissolution of α-MnO_2 and markedly improved the conductivity for AZIBs. Furthermore, the interplay between hydroxylated interphase on the surface and the unique bivalence structure of Mn_5O_8 suppresses the gas evolution reactions and provides the facile pathway for ion transport via intra-/inter-layer defects of Mn_5O_8 (Shan et al. 2016). Recently, MnO_x@N-C was used as the cathode and indicated that onion-like N-doped carbon and amorphous carbon shell contributed to a high reversibly capacity and cyclic stability for rechargeable aqueous zinc-ion batteries (Fu et al. 2018).

A series of approaches have been studied to enhance the electrochemical performances of MnO_2/zinc salts/Zn battery system. For instance, the electrical conductivity of the MnO_2 electrode was improved by doping carbons (Hu et al. 2017; Zeng et al. 2017; Huang et al. 2018). Owing to its higher electronegativity (3.04) and smaller atomic diameter, N-doped carbon matrix is promising material and made a lot of gains (Fu et al. 2018). Herein, a special β-MnO_2/N-doped carbon matrix (NCm) composites and Mn_5O_8/NCm composites were effectively prepared throughout one-pot hydrothermal method, and polyaniline (PANI) by heating was used as the sources of carbon and nitrogen. This study provides insights necessary to design other metal oxides/NCm materials for AZIBs and other cost-effective and environmentally friendly battery systems.

Experimental

Materials synthesis

MnOOH/PANI precursor was synthesized via a one-step hydrothermal method. First of all, 3 mmol of $MnSO_4{\cdot}H_2O$ and 0.5 mol L^{-1} of H_2SO_4 (2 mL) were transferred into 60 mL of deionized water, and magnetically agitated until a clear solution was obtained. Next, 0.1 mol $KMnO_4$ (20 mL) aqueous solution was slowly dropped into the above mixture to form a dark violet solution. Then, the mixed solution was agitated for 2 h at room temperature. And then, 50 μL of aniline was slowly dropped into the solution and continued to stir for 2 h. At last, 0.125 g of $(NH_4)_2S_2O_8$ was added into the mixture. After agitating for another 30 min, the mixture was poured to 110 mL of Teflon-lined stainless steel autoclave and heated at 120 °C for 12 h. The precursor was obtained by centrifugation after cooling, washed with deionized water and ethanol three times, and dried by vacuum drying oven. The β-MnO_2/NCm was prepared through heating at 300 °C for 2 h in air atmosphere. The Mn_5O_8/NCm was prepared through heating at 500 °C for 4 h in air atmosphere. The synthesis route of MnOOH/PANI precursor is shown in Scheme 1. Likewise, the β-MnO_2 powders were also synthesized with a similar method without the polymerization with PANI.

Materials characterization

The morphologies were characterized by scanning electron microscope (SEM, ZEISS SUPRATM 55). The prepared samples were characterized by X-ray diffraction (XRD, SHMADZUXRD-6100AS) with Cu Kα radiation (λ = 1.5418 Å). Transmission electron microscope (TEM) and energy-dispersive X-ray spectroscopy (EDS) were obtained using Tecnai G2F30 S-Twin operated at 300 kV. X-ray photoelectron spectroscopy (XPS) measurements were performed on an ESCALAB 250 spectrometer with Mg Kα X-ray source.

Electrochemical measurements

The 2032 coin-type cells were assembled in open air atmosphere to evaluate the electrochemical performance with a Neware BTS-4008 battery test system. The electrochemical properties were investigated using products as cathode, zinc foil as anode, filter paper as the

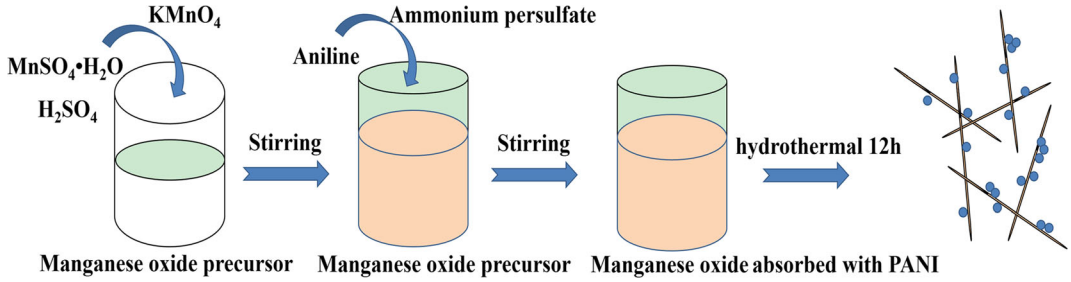

Scheme 1 Schematic illustration of the fabrication process of MnOOH/PANI precursor

separator, and 1 mol L^{-1} $ZnSO_4$ aqueous solution as electrolyte. To prepare the cathode, the homemade products, acetylene black, and polyvinylidene fluoride were mixed in a weight ratio of 8/1/1, and the mixture was dispersed in N-methyl-2-pyrrolidone to form a stable homogeneous slurry. Then, the mixture was cast on stainless steel foil and dried overnight under vacuum conditions at 110 °C. An active material loading of around 1.0 mg cm^{-2} was used, and the diameter of zinc foil was 12 mm. The simulated cells were cycled at room temperature within the voltage range of 1.00–1.85 V (vs. Zn/Zn^{2+}). Cyclic voltammograms (CV) and electrochemical impedance spectroscopy (EIS) were performed on a CHI660E electrochemical workstation at room temperature. The EIS were tested at the frequency range 0.01 Hz–100 kHz with alternating-current voltage of 5 mV.

Results and discussion

The SEM and XRD were carried out to identify the microstructure of the MnOOH/PANI intermediate, β-MnO_2/NCm composites, and Mn_5O_8/NCm composites. SEM image of the MnO_2 (Supplementary Fig. S1) demonstrates a homogeneous one-dimensional nanorod structure. After reacting with PANI, the surface of the nanorod is coated with numerous PANI nanoparticle, and the size of MnOOH/PANI intermediate is 80~200 nm (Fig. 1a). The XRD pattern of the precursor in Fig. 1b exhibits that all peaks can be assigned to MnOOH (JCPDS 41-1379). Owing to PANI was amorphous, and PANI was not detected in the XRD pattern of MnOOH/PANI. The morphology of the precursor does not change after heat treatment at 300 °C (Fig. 1c) or 500 °C (Fig. 1e) for 4 h in air during the process of the formation of MnO_2 and Mn_5O_8. The XRD results of the products suggest that all peaks can be assigned to β-MnO_2 (JCPDS 24-0735, Fig. 1d) and Mn_5O_8 (JCPDS 39-1218, Fig. 1f) during calcination, respectively.

The TEM provides more details about the β-MnO_2/NCm composites. Figure 2a demonstrates that N-doped carbon nanoparticles are tied to β-MnO_2 nanorod, which is corresponded with Fig. 1c. The HAADF-STEM and EDX analysis were used to further confirm the element distribution of the β-MnO_2/NCm composites (Fig. 2b–g). The EDX mapping of the β-MnO_2/NCm composites shows the homogeneous distribution of C (Fig. 2d), Mn (Fig. 2e), O (Fig. 2f), and N (Fig. 2g), respectively. The EDX results imply that C and N element are the homogeneous distribution of β-MnO_2/NCm. The survey on XPS spectra of β-MnO_2/NCm composites indicates the existence of C, Mn, O, and N elements in Fig. 2h, which is in accordance with the EDX mapping result (Fig. 2b–g). The typical high-resolution spectrum of C 1s in Fig. 2i includes four peaks, which locate at 284.4, 285.1, 286.4, and 288.2 eV in consistent with C–C, C–N, C–O, and O=C–O, respectively (Li et al. 2017; Ren et al. 2017). From the spectrum of Mn 2p (Fig. 2j) reveals two peaks (642.2 and 653.9 eV), which are in accordance with the characteristic Mn $2p_{3/2}$ and Mn $2p_{1/2}$ binding energies of MnO_2, with the spin energy separation of 11.7 eV (Liu et al. 2010; Thirupathi and Smirniotis 2012). The spectrum of O 1s is presented in Fig. 2k, in which two peaks at 529.8 and 531 eV are ascribed to Mn–O–Mn and Mn–O–H, respectively (Wang et al. 2013a, b). The XPS survey spectrum of N 1s is shown in Supplementary Fig. S2.

The TEM image of Mn_5O_8/NCm composites is shown in Fig. 3a. The element distribution of Mn_5O_8/NCm was observed with HAADF-STEM and EDX analysis (Fig. 3b–g). EDX results show the homogeneous distribution of C, Mn, O, and N element in Mn_5O_8/NCm (Fig. 3d–g). The Mn_5O_8/NCm has been analyzed by XPS as shown in Fig. 3h, and the XPS result is in accordance with the EDX mapping result

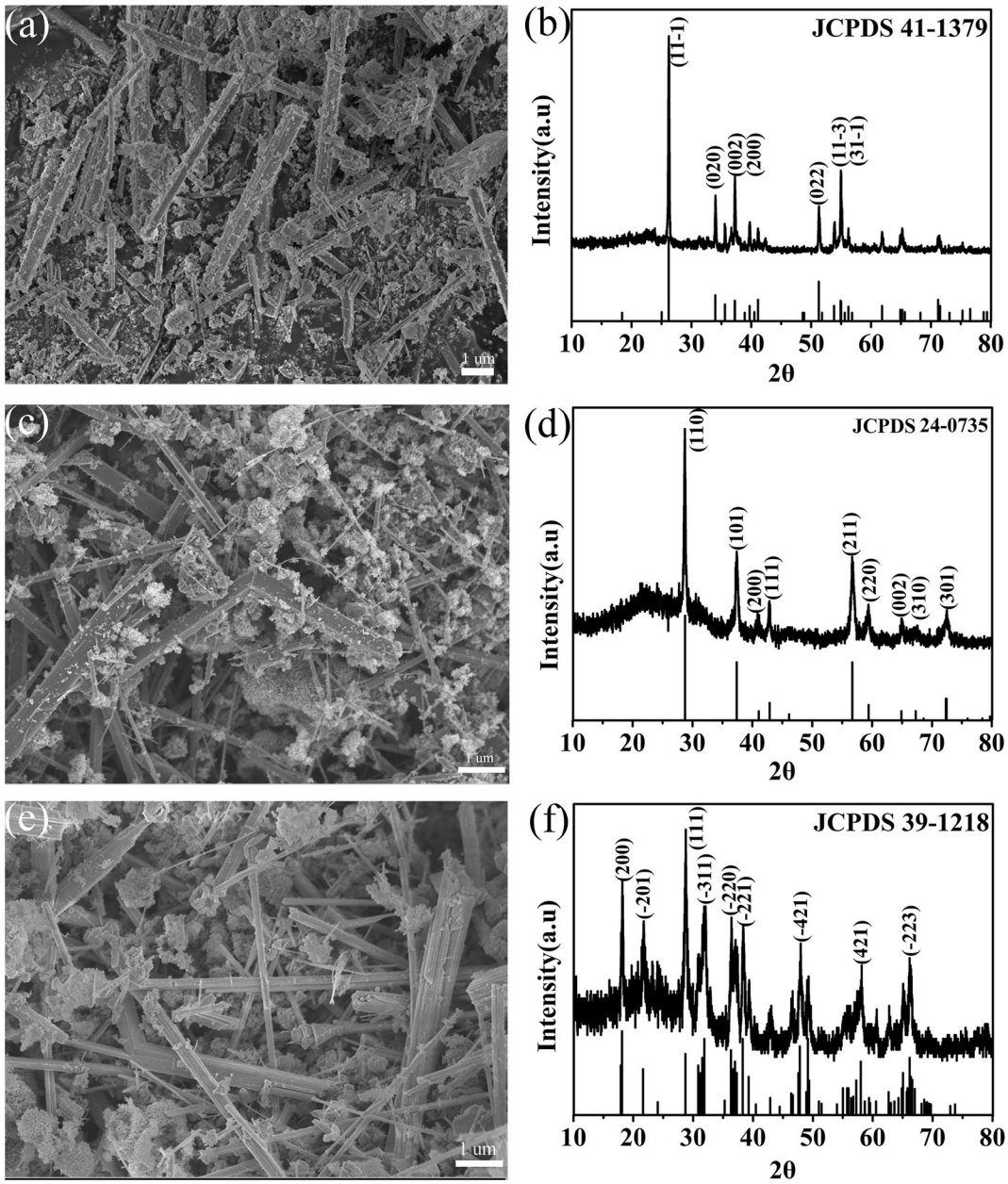

Fig. 1 SEM images (**a**) and XRD pattern (**b**) of the MnOOH/PANI precursor. SEM images (**c**) and XRD (**d**) pattern of the β-MnO_2/NCm composites. SEM images (**e**) and XRD (**f**) pattern of the Mn_5O_8/NCm composites

(Fig. 3b–g). The C 1s spectrum of Mn_5O_8/NCm composites is shown in Fig. 3i and four peaks at 285.9 eV, 285.4 eV, 285.7 eV, and 284.4 eV (Ren et al. 2017; Qiu et al. 2018a, b). As recorded in Fig. 3j, the spectrum of Mn 2p shows two peaks at 642.1 and 653.9 eV which ascribe to Mn $2p_{3/2}$ and Mn $2p_{1/2}$, respectively (Liu et al. 2015). The O 1s photoelectron spectrum (Fig. 3k) of the Mn_5O_8/NCm nanorod shows two peaks at about 530.0 and 531.8 eV (Gao et al. 2010). The high-resolution spectrum of N1s is shown in Supplementary Fig. S3.

To research the electrochemical performance of the β-MnO_2/NCm and Mn_5O_8/NCm, CV and galvanostatic discharge/charge measurement were executed. Figure 4a shows the CV profiles of β-MnO_2/NCm composites cathodes. The CV curves of β-MnO_2/NCm reduction/oxidation peaks located at 1.22/1.38

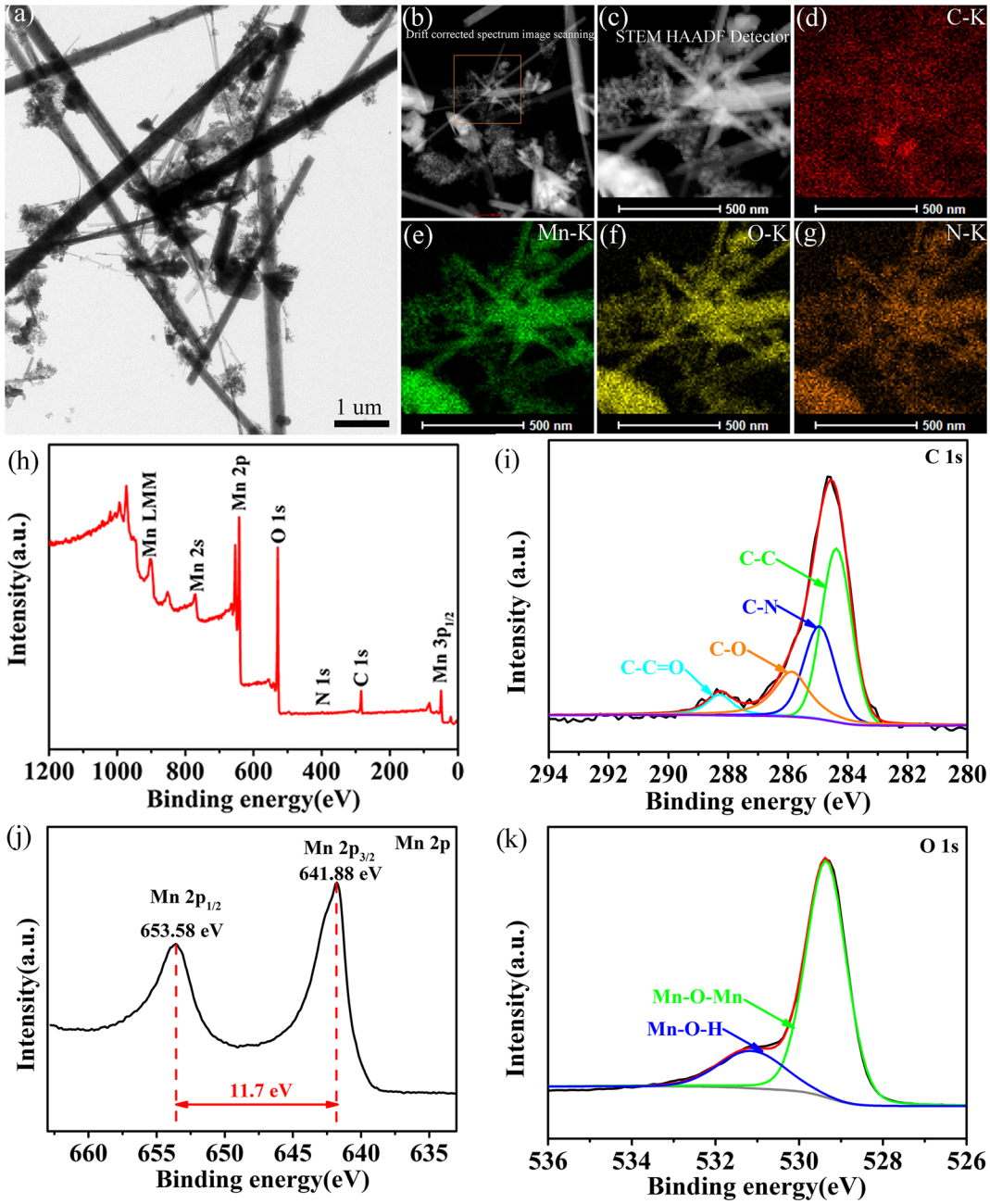

Fig. 2 TEM image of β-MnO_2/NCm composites (**a**). Drift corrected spectrum image scanning (**b**) and HAADF-STEM image of β-MnO_2/NCm composites (**c**). EDX elemental mapping images of C (**d**) Mn (**e**), O (**f**), and N (**g**). XPS wide spectrum of β-MnO_2/NCm composites (**h**), C 1s (**i**), Mn 2p (**j**), and O 1s (**k**) in the composites

and 1.56 V, and the β-MnO_2 peaks located at 1.23/1.39 and 1.62 V (Supplementary Fig. S4), indicating a similar redox behavior. The peaks at 1.22 and 1.38 V for β-MnO_2/NCm composites can be ascribed to the insertion of H^+ and Zn^{2+} into the β-MnO_2/NCm composites, corresponded with the reduction of Mn^{4+} to Mn^{3+} (Huang et al. 2018). In contrast, the peak at 1.56 V for β-MnO_2/NCm composites corresponds to the extraction of Zn^{2+}, which involves the reversible oxidation of Mn^{3+} to Mn^{4+} (Alfaruqi et al. 2015a, b; Islam et al. 2017a, b). The electrochemical properties of the Mn_5O_8/NCm composites cathodes are assessed using

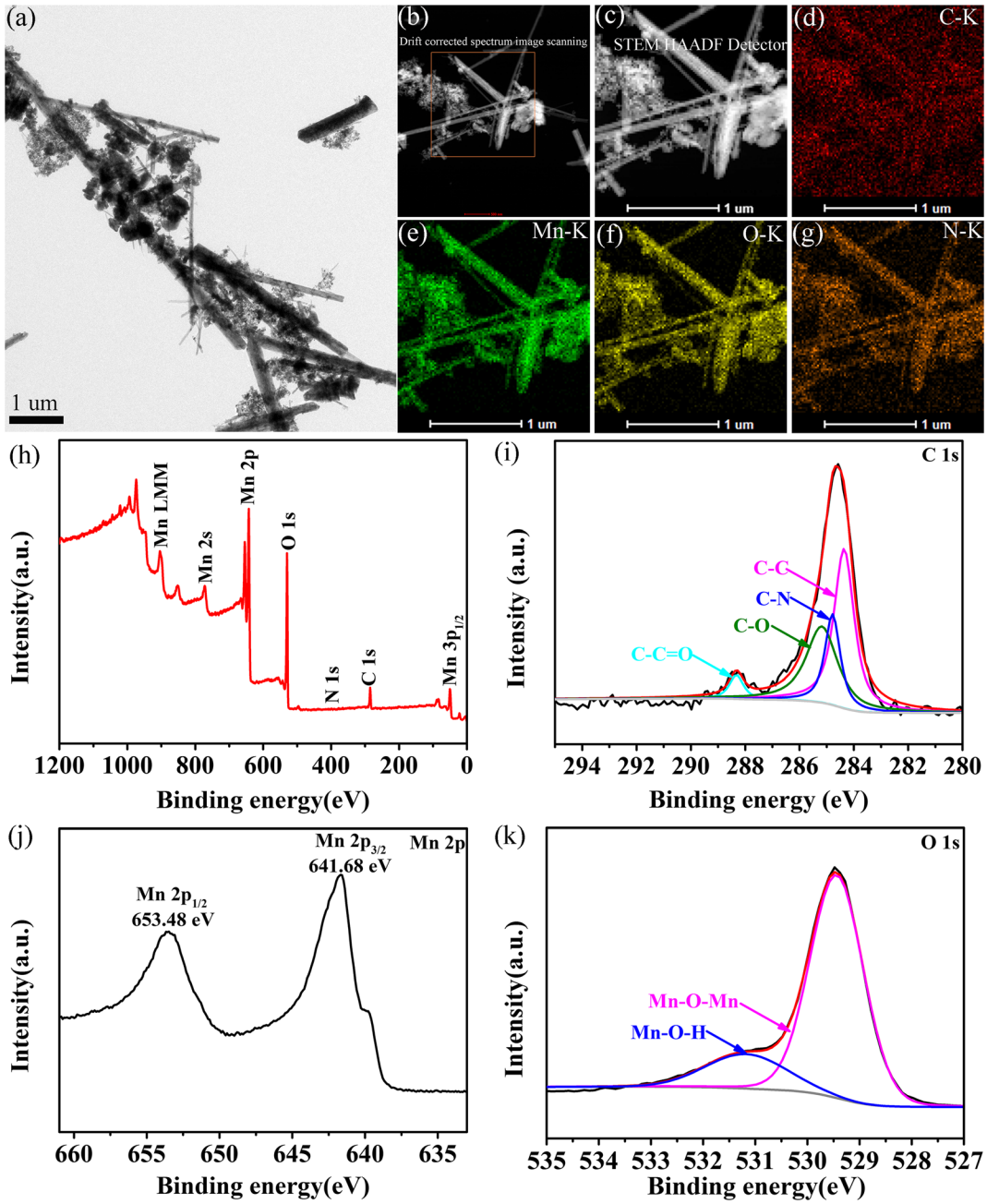

Fig. 3 TEM image of Mn_5O_8/NCm composites (**a**). Drift corrected spectrum image scanning (**b**) and HAADF-STEM image of Mn_5O_8/NCm composites (**c**). EDX elemental mapping images of C (**d**) Mn (**e**), O (**f**), and N (**g**). XPS wide spectrum of Mn_5O_8/NCm composites (**h**), C 1s (**i**), Mn 2p (**j**), and O 1s (**k**) in the composites

CV as shown in Fig. 4b. The CV curves of Mn_5O_8/NCm ($Mn^{2+}{}_2Mn^{4+}{}_3O_8$) show that sharp anodic peak centered at about 1.67 V and two cathodic peaks at 1.20 and 1.33 V are related to extraction/insertion of Zn^{2+} and H^+ (Hao et al. 2018). Figure 4c shows that the discharge/charge profiles of the β-MnO_2/NCm composite electrode compare with that obtained for the β-MnO_2 electrode at 200 mA g^{-1}. The β-MnO_2/NCm electrode delivered a higher discharge capacity of 331 mAh g^{-1} comparing with 185 mAh g^{-1} for the pure β-MnO_2 electrode in a 2 M $ZnSO_4$ aqueous electrolyte (Alfaruqi et al. 2017). After 100th cycles, the capacity

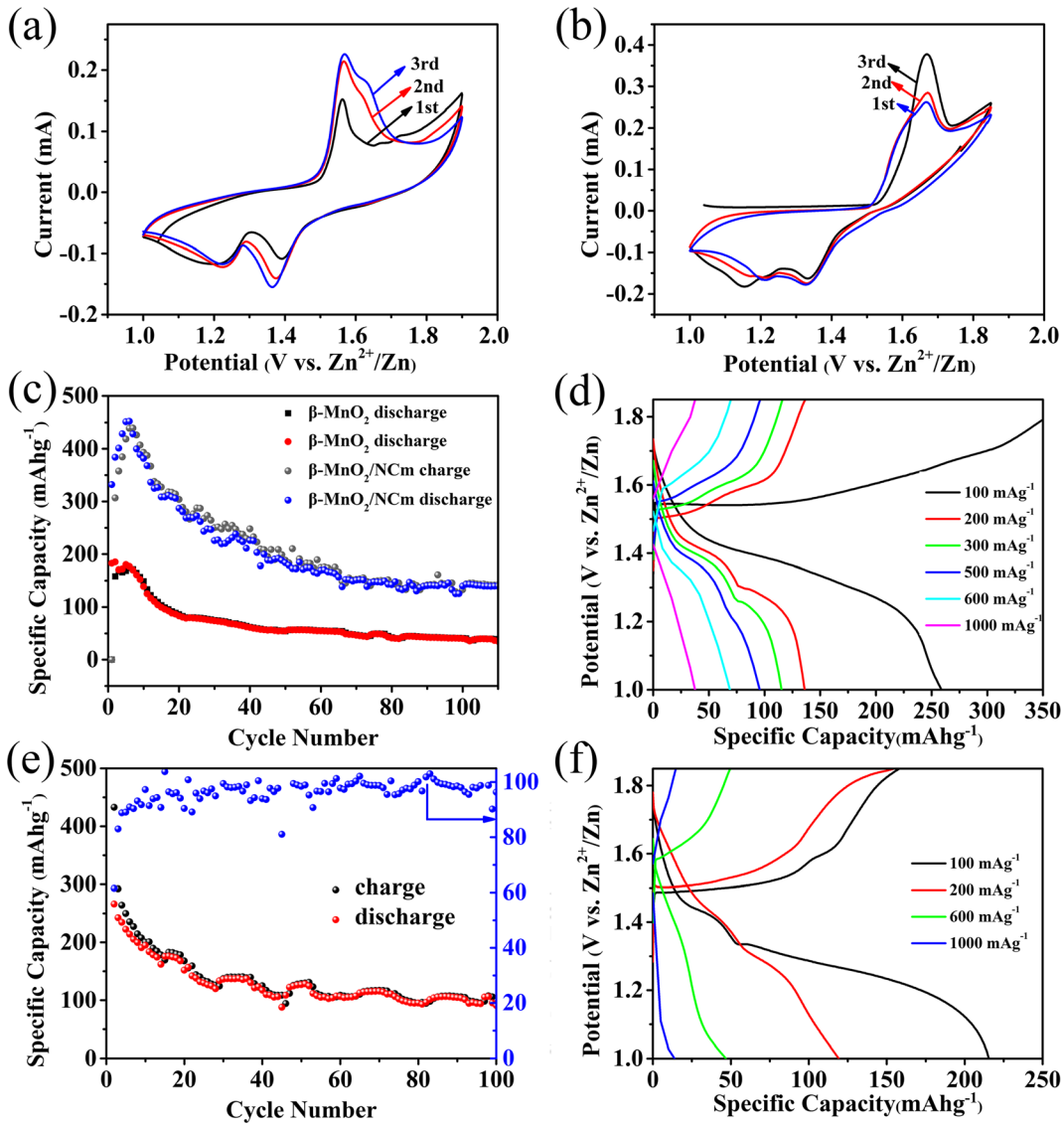

Fig. 4 CV curves of the β-MnO_2/NCm (**a**). Cycling performance of the β-MnO_2/NCm at 200 mA g^{-1} (**c**). Rate performance of β-MnO_2/NCm at different current densities (**d**). CV curves of the Mn_5O_8/NCm (**b**). Cycling performance of the Mn_5O_8/NCm at 200 mA g^{-1} (**e**). Rate performance of Mn_5O_8/NCm at different current densities (**f**)

of 143.7 mAh g^{-1} is retained for the β-MnO_2/NCm electrode than that of the bare β-MnO_2 electrode (40.7 mAh g^{-1}) in a 2 M $ZnSO_4$ aqueous electrolyte. The N-doped carbon-coated samples can accommodate more Zn^{2+} ions than the uncoated MnO_2 (Islam et al. 2017a, b). The cycling performance of bare β-MnO_2 electrode, shown in Supplementary Fig. S5, indicates that the capacity of the bare β-MnO_2 electrode (120.5 mAh g^{-1}) with 0.1 M $MnSO_4$ additive in a 2 M $ZnSO_4$ aqueous electrolyte at 200 mA g^{-1} is slightly lower than that of reported in literature (~ 135 mAh g^{-1}, Islam et al. 2017a, b). The N-doped carbon and the additional $MnSO_4$ in electrolyte can improve of the capacity in the β-MnO_2 electrode. After the initial cycle, the increase in capacity is owing to the activation of electrode (Islam et al. 2017a). The β-MnO_2/NCm and β-MnO_2 electrode show a gradual fading in capacity which results from manganese dissolution in electrolyte (Alfaruqi et al. 2015a, b). The electrochemical property is further corroborated in the rate performances (Fig. 4d). The cell shows an excellent rate capability, achieving high capacities of 258, 136, 115, 95, 68, and

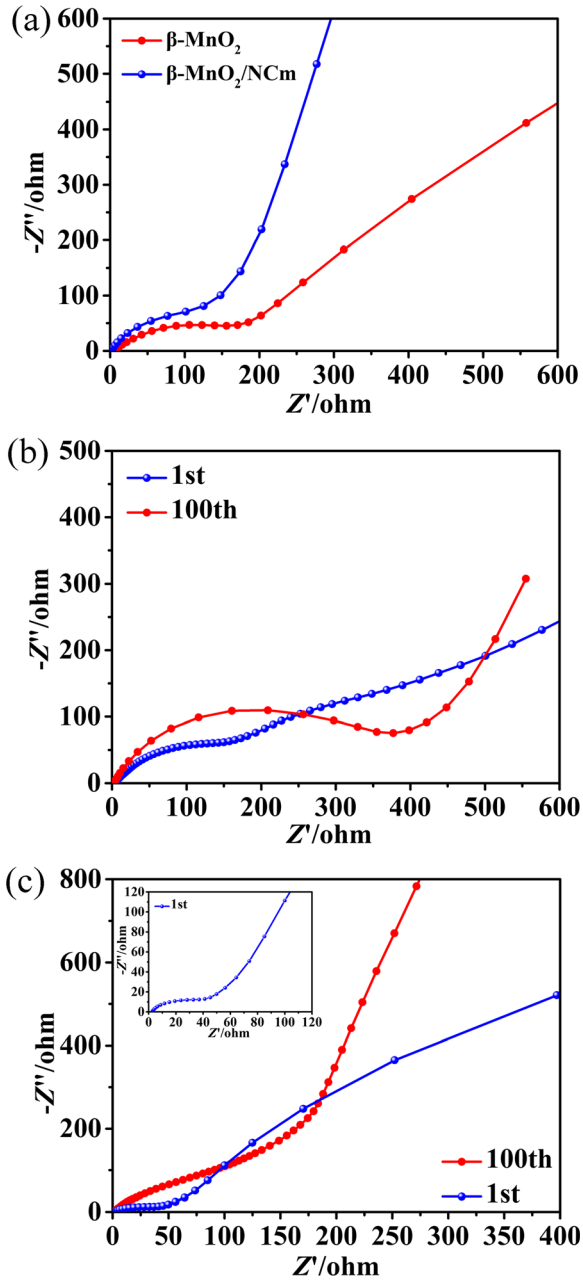

Fig. 5 Nyquist plots of β-MnO_2/NCm hybrid composites and pure β-MnO_2 electrodes (**a**). Nyquist plots of the β-MnO_2/NCm composites before the first cycle and after 100th cycles (**b**). Nyquist plots of the Mn_5O_8/NCm composites before the first cycle and after 100th cycles (**c**)

37 mAh g^{-1} at 100, 200, 300, 500, 600, and 1000 mA g^{-1}, respectively. The rate performances of β-MnO_2/NCm electrode are lower than the additional $MnSO_4$ in electrolyte. The results above indicate that manganese oxides/N-doped carbon matrix composites are promising for a high-performance and cost-effective battery system.

Figure 5 illustrates the EIS results of β-MnO_2/NCm composites and Mn_5O_8/NCm composites. The spectrum contains a semicircle and straight sloping line which correspond to the Faradaic reaction and the charge transfer resistance impedance (R_{ct}), respectively (Alfaruqi et al. 2017). The diameter of the semicircle for the β-MnO_2/NCm cathode is smaller than that of the β-MnO_2 cathode, suggesting lower charge-transfer impedance in β-MnO_2/NCm composites (Fig. 5a). The lower charge-transfer impedance of β-MnO_2/NCm is ascribed to the co-effect of N-doping and carbon material which increase the conductivity significantly (Ren et al. 2017). EIS results demonstrate the steeper slope of β-MnO_2/NCm, suggesting rapid Zn^{2+} diffusion in β-MnO_2/NCm electrode. The calculated R_{ct} value of the β-MnO_2/NCm electrodes was 142.7 Ω and increased to 377 Ω after 100 cycles (Fig. 5b). Figure 5c illustrates that the calculated R_{ct} value (40 Ω) of the Mn_5O_8/NCm was lower than that of the β-MnO_2/NCm. After 100 cycles, the calculated R_{ct} value of the Mn_5O_8/NCm electrodes was 167 Ω. During the consistent discharge/charge processes, the pathways for Zn^{2+} insertion/extraction in manganese oxides/NCm composites deconstructed, which may result in the mild raise of the resistances (Wu et al. 2018a, b).

Conclusions

In summary, the metal oxides/NCm composites electrodes were synthesized for use as cathodes in AZIB via a one-pot hydrothermal method combining with heat treatment. The β-MnO_2/NCm electrode registered a higher capacity than the β-MnO_2 electrode. Ascribing to the N-doped carbon matrix, the β-MnO_2/NCm composites exhibited high discharge capacity and stable cycle performance for AZIB. By the similar process of preparation, Mn_5O_8/NCm composites can deliver 266 mAh g^{-1} at current densities of 200 mA g^{-1}. Compare to β-MnO_2/NCm composites, Mn_5O_8/NCm composites have superior electrical conductivity and lower reversible capacities. The synthesis process showed in this paper provides an effective and facile way to develop other oxides/NCm composites for AZIBs and other cost-effective and environmentally friendly battery systems.

Funding information The work described in this paper was supported by Shandong Province Natural Science Foundation (ZR2012EMM009, ZR2013EMQ005 and ZR2018MEM012), the Foundation of Key Laboratory of Pulp and Paper Science and Technology of Ministry of Education/Shandong Province of China (No. KF201602), the Scientific Research Foundation for the Returned Overseas Scholars in Jinan (20100406), National Training Program of Innovation and Entrepreneurship for Undergraduates (201610431033 and 201810431008), and National Natural Science Foundations of China (31570566, 31500489, 51372140, 51303086, 51403111, 51503107, and 51172130).

Compliance with ethical standards

Conflict of interest The authors declare that they have no conflict of interest.

Publisher's note Springer Nature remains neutral with regard to jurisdictional claims in published maps and institutional affiliations.

References

Alfaruqi MH, Gim J, Kim S, Song J, Jo J, Kim S, Mathew V, Kim J (2015a) Enhanced reversible divalent zinc storage in a structurally stable α-MnO_2 nanorod electrode. J Power Sources 288:320–327. https://doi.org/10.1016/j.jpowsour.2015.04.140

Alfaruqi MH, Mathew V, Gim J, Kim S, Song J, Baboo JP, Choi SH, Kim J (2015b) Electrochemically induced structural transformation in a γ-MnO_2 cathode of a high capacity zinc-ion battery system. Chem Mater 27:3609–3620. https://doi.org/10.1021/cm504717p

Alfaruqi MH, Islam S, Mathew V, Song J, Kim S, Tung DP, Jo J, Kim S, Baboo JP, Xiu Z, Kim J (2017) Ambient redox synthesis of vanadium-doped manganese dioxide nanoparticles and their enhanced zinc storage properties. Appl Surf Sci 404:435–442. https://doi.org/10.1016/j.apsusc.2017.02.009

Boeun Lee HRS, Lee HR, Yoon CS, Kim JH, Chung KY, Cho BW, Oh SH (2016) Critical role of pH evolution of electrolyte in the reaction mechanism for rechargeable zinc batteries. ChemSusChem 9:2948–2956. https://doi.org/10.1002/cssc.201600702

Bruce PG, Freunberger SA, Hardwick LJ, Tarascon JM (2012) Li-O_2 and Li-S batteries with high energy storage. Nat Mater 11:19–29. https://doi.org/10.1038/NMAT3191

Cao K, Liu H, Li Y, Wang Y, Jiao L (2017) Encapsulating sulfur in δ-MnO_2 at room temperature for Li-S battery cathode. Energy Storage Mater 9:78–84. https://doi.org/10.1016/j.ensm.2017.06.012

Chang L, Feng L, Lai-Peng M, Hui-Ming C (2010) Advanced materials for energy storage. Adv Mater 22:E28–E62. https://doi.org/10.1002/adma.200903328

Dunn B, Kamath H, Tarascon JM (2011) Electrical energy storage for the grid: a battery of choices. Science 334:928–935. https://doi.org/10.1126/science.1212741

Fu Y, Wei Q, Zhang G, Wang X, Zhang J, Hu Y, Wang D, Zuin L, Zhou T, Wu Y, Sun S (2018) High-performance reversible aqueous Zn-ion battery based on porous MnO_x Nanorods coated by MOF-derived N-doped carbon. Adv Energy Mater 8:1801445. https://doi.org/10.1002/aenm.201801445

Gao T, Norby P, Krumeich F, Okamoto H, Nesper R, Fjellvåg H (2010) Synthesis and properties of layered-structured Mn_5O_8 Nanorods. J Phys Chem C 114:922–928. https://doi.org/10.1021/jp9097606

Hao J, Mou J, Zhang J, Dong L, Liu W, Xu C, Kang F (2018) Electrochemically induced spinel-layered phase transition of Mn_3O_4 in high performance neutral aqueous rechargeable zinc battery. Electrochim Acta 259:170–178. https://doi.org/10.1016/j.electacta.2017.10.166

He P, Yan M, Zhang G, Sun R, Chen L, An Q, Mai L (2017) Layered VS_2 Nanosheet-based aqueous Zn ion battery cathode. Adv Energy Mater 7:1601920. https://doi.org/10.1002/aenm.201601920

Hu P, Yan M, Wang X, Han C, He L, Wei X, Niu C, Zhao K, Tian X, Wei Q, Li Z, Mai L (2016) Single-nanowire electrochemical probe detection for internally optimized mechanism of porous graphene in electrochemical devices. Nano Lett 16:1523–1529. https://doi.org/10.1021/acs.nanolett.5b03576

Hu P, Yan M, Zhu T, Wang X, Wei X, Li J, Zhou L, Li Z, Chen L, Mai L (2017) Zn/V_2O_5 aqueous hybrid-ion battery with high voltage platform and long cycle life. ACS Appl Mater Interfaces 9:42717–42722. https://doi.org/10.1021/acsami.7b13110

Hu P, Zhu T, Wang X, Wei X, Yan M, Li J, Luo W, Yang W, Zhang W, Zhou L, Zhou Z, Mai L (2018) Highly durable $Na_2V_6O_{16}.1.63H_2O$ nanowire cathode for aqueous zinc-ion battery. Nano Lett 18:1758–1763. https://doi.org/10.1021/acs.nanolett.7b04889

Huang J, Wang Z, Hou M, Dong X, Liu Y, Wang Y, Xia Y (2018) Polyaniline-intercalated manganese dioxide nanolayers as a high-performance cathode material for an aqueous zinc-ion battery. Nat Commun 9:2906. https://doi.org/10.1038/s41467-018-04949-4

Islam S, Alfaruqi MH, Mathew V, Song J, Kim S, Kim S, Jo J, Baboo JP, Pham DT, Putro DY, Sun Y-K, Kim J (2017a) Facile synthesis and the exploration of the zinc storage mechanism of β-MnO_2 nanorods with exposed (101) planes as a novel cathode material for high performance eco-friendly zinc-ion batteries. J Mater Chem A 5:23299–23309. https://doi.org/10.1039/C7TA07170A

Islam S, Alfaruqi MH, Song J, Kim S, Pham DT, Jo J, Kim S, Mathew V, Baboo JP, Xiu Z, Kim J (2017b) Carbon-coated manganese dioxide nanoparticles and their enhanced electrochemical properties for zinc-ion battery applications. J Energy Chem 26:815–819. https://doi.org/10.1016/j.jechem.2017.04.002

Jiang J, Li Y, Liu J, Huang X, Yuan C, Lou XW (2012) Recent advances in metal oxide-based electrode architecture design for electrochemical energy storage. Adv Mater 24:5166–5180. https://doi.org/10.1002/adma.201202146

Li F, Ren M, Liu W, Li G, Li M, Su L, Gao C, Hei J, Yang H (2017) Sea urchin-like CoO/co/N-doped carbon matrix hybrid composites with superior high-rate performance for lithium-ion batteries. J Alloys Compd 701:524–532. https://doi.org/10.1016/j.jallcom.2017.01.144

Liu R, Duay J, Lee SB (2010) Redox exchange induced MnO_2 nanoparticle enrichment in poly(3,4-ethylenedioxythiophene)

nanowires for electrochemical energy storage. ACS Nano 4: 4299–4307. https://doi.org/10.1021/nn1010182

Liu G, Hall J, Nasiri N, Gengenbach T, Spiccia L, Cheah MH, Tricoli A (2015) Scalable synthesis of efficient water oxidation catalysts: insights into the activity of flame-made manganese oxide nanocrystals. ChemSusChem 8:4162–4171. https://doi.org/10.1002/cssc.v8.17/issuetoc

Lund H (2007) Renewable energy strategies for sustainable development. Energy 32:912–919. https://doi.org/10.1016/j.energy.2006.10.017

Qiu N, Chen H, Yang Z, Sun S, Wang Y (2018a) Low-cost birnessite as a promising cathode for high-performance aqueous rechargeable batteries. Electrochim Acta 272:154–160. https://doi.org/10.1016/j.electacta.2018.04.012

Qiu Z, Peng Y, He D, Wang Y, Chen S (2018b) Ternary Fe_3O_4@C@PANi nanocomposites as high-performance supercapacitor electrode materials. J Mater Sci 53:12322–12333. https://doi.org/10.1007/s10853-018-2451-9

Ren M, Xu H, Li F, Liu W, Gao C, Su L, Li G, Hei J (2017) Sugarapple-like N-doped TiO_2 @carbon core-shell spheres as high-rate and long-life anode materials for lithium-ion batteries. J Power Sources 353:237–244. https://doi.org/10.1016/j.jpowsour.2017.04.015

Sambandam B, Soundharrajan V, Kim S, Alfaruqi MH, Jo J, Kim S, Mathew V, Sun Y-k, Kim J (2018) Aqueous rechargeable Zn-ion batteries: an imperishable and high-energy $Zn_2V_2O_7$ nanowire cathode through intercalation regulation. J Mater Chem A 6:3850–3856. https://doi.org/10.1039/c7ta11237h

Senguttuvan P, Han S-D, Kim S, Lipson AL, Tepavcevic S, Fister TT, Bloom ID, Burrell AK, Johnson CS (2016) A high power rechargeable nonaqueous multivalent Zn/V_2O_5 battery. Adv Energy Mater 6:1600826. https://doi.org/10.1002/aenm.201600826

Shan X, Charles DS, Lei Y, Qiao R, Wang G, Yang W, Feygenson M, Su D, Teng X (2016) Bivalence Mn_5O_8 with hydroxylated interphase for high-voltage aqueous sodium-ion storage. Nat Commun 7:13370. https://doi.org/10.1038/ncomms13370

Suo L, Borodin O, Gao T, Olguin M, Ho J, Fan X, Luo C, Wang C, Xu K (2015) "Water-in-salt" electrolyte enables high-voltage aqueous lithium-ion chemistries. Science 350:938–943. https://doi.org/10.1126/science.aab1595

Tarascon JM, Armand M (2001) Issues and challenges facing rechargeable lithium batteries. Nature 414:359. https://doi.org/10.1038/35104644

Thirupathi B, Smirniotis PG (2012) Nickel-doped Mn/TiO_2 as an efficient catalyst for the low-temperature SCR of NO with NH_3: catalytic evaluation and characterizations. J Catal 288: 74–83. https://doi.org/10.1016/j.jcat.2012.01.003

Trocoli R, La Mantia F (2015) An aqueous zinc-ion battery based on copper hexacyanoferrate. ChemSusChem 8:481–485. https://doi.org/10.1002/cssc.201403143

Wang G, Tang Q, Bao H, Li X, Wang G (2013a) Synthesis of hierarchical sulfonated graphene/MnO_2/polyaniline ternary composite and its improved electrochemical performance. J Power Sources 241:231–238. https://doi.org/10.1016/j.jpowsour.2013.04.122

Wang B, Wang Y, Sun B, Munroe P, Wang G (2013b) Coral-like V_2O_5 nanowhiskers as high-capacity cathode materials for lithium-ion batteries. RSC Adv 3:5069. https://doi.org/10.1039/c3ra22425b

Wei T, Li Q, Yang G, Wang C (2018) An electrochemically induced bilayered structure facilitates long-life zinc storage of vanadium dioxide. J Mater Chem A 6:8006–8012. https://doi.org/10.1039/C8TA02090F

Wu S, Wang Y, Liu W-L, Ren M, Kong F-G, Wang S-J, Wang X, Zhao H, Bao J-M (2018a) A high-capacity and long-life aqueous rechargeable zinc battery using porous metal–organic coordination polymers nanosheets cathode. Inorg Chem Front. https://doi.org/10.1039/C8QI00959G

Wu B, Zhang G, Yan M, Xiong T, He P, He L, Xu X, Mai L (2018b) Graphene scroll-coated alpha-MnO_2 nanowires as high-performance cathode materials for aqueous Zn-ion battery. Small 14:e1703850. https://doi.org/10.1002/smll.201703850

Xia C, Guo J, Lei Y, Liang H, Zhao C, Alshareef HN (2018a) Rechargeable aqueous zinc-ion battery based on porous framework zinc pyrovanadate intercalation cathode. Adv Mater 30:1705580. https://doi.org/10.1002/adma.201705580

Xia J, Zhu F, Wang L, Wang G, Meng Y, Zhang Y (2018b) In situ coating on $LiFePO_4$ with ionic liquid as carbon source for high-performance lithium batteries. J Nanopart Res 20:196. https://doi.org/10.1007/s11051-018-4298-z

Xu C, Li B, Du H, Kang F (2012) Energetic zinc ion chemistry: the rechargeable zinc ion battery. Angew Chem 51:933–935. https://doi.org/10.1002/ange.201106307

Yan M, He P, Chen Y, Wang S, Wei Q, Zhao K, Xu X, An Q, Shuang Y, Shao Y, Mueller KT, Mai L, Liu J, Yang J (2018) Water-lubricated intercalation in V_2O_5 .nH_2O for high-capacity and high-rate aqueous rechargeable zinc batteries. Adv Mater 30:1703725. https://doi.org/10.1002/adma.201703725

Zeng Y, Zhang X, Meng Y, Yu M, Yi J, Wu Y, Lu X, Tong Y (2017) Achieving ultrahigh energy density and long durability in a flexible rechargeable quasi-solid-state Zn-MnO_2 battery. Adv Mater 29:1700274. https://doi.org/10.1002/adma.201700274

Zhai Y, Dou Y, Zhao D, Fulvio PF, Mayes RT, Dai S (2011) Carbon materials for chemical capacitive energy storage. Adv Mater 23:4828–4850. https://doi.org/10.1002/adma.201100984

Zhang L, Chen L, Zhou X, Liu Z (2015) Towards high-voltage aqueous metal-ion batteries beyond 1.5 V: the zinc/zinc Hexacyanoferrate system. Adv Energy Mater 5:1400930. https://doi.org/10.1002/aenm.201400930

Zhang H, Wang Y-F, Liu W-L, Kong F-G, Ren M-M, Wang S-J, Wang X-Q, Duan X-L, Peng D (2018) Designed synthesis of CoO/CuO/rGO ternary nanocomposites as high-performance anodes for lithium-ion batteries. JOM 70:1793–1799. https://doi.org/10.1007/s11837-018-2801-8

Zhao S, Han B, Zhang D, Huang Q, Xiao L, Chen L, Ivey DG, Deng Y, Wei W (2018) Unravelling the reaction chemistry and degradation mechanism in aqueous Zn/MnO_2 rechargeable batteries. J Mater Chem A 6:5733–5739. https://doi.org/10.1039/c8ta01031e